Novel Composite Inorganic Ceramic Membranes for Gas Separations and Environmental Applications

Shehu Habiba, Okon Edidiong and Edward Gobina

Abstract Composite ceramic inorganic membranes have been prepared using different types of support with the aim to achieving high selectivity for lower hydrocarbons. Upon modification of the support, the morphology was examined using Scanning Electron Microscopy (SEM), which showed a reduction in the pore radius and pore size distribution. Energy Dispersive X-ray Diffraction (EDAX) was used to determine the elemental composition of the membrane. Gas permeation tests were carried out with inorganic ceramic membrane consisting of a ceramic support and a zeolite layer. The permeance of nitrogen, carbon dioxide, helium, methane, propane and argon through the membrane at varying pressures was determined. The effect of the mean pressure of up to 0.1 MPa on the molar flux of the gases at 294 K was determined.

Keywords Characterization · Composite membranes · Knudsen flow · Permeability · Permeance · Selectivity

Nomenclatures

Symbols

E_{diff}	Activation energy (J mol^{-1})
E_e	Activation energy for activated gas translational diffusion (J mol^{-1})
D_∞	Arrhenius-type pre-exponential factor (m^2 s^{-1})
$\bar{P}$	Average pressure drop across the membrane (Pa)
B	Constant representing Knudsen flow

S. Habiba · O. Edidiong · E. Gobina (✉)
School of Engineering, Centre for Process Integration and Membrane Technology (CPIMT), The Robert Gordon University Aberdeen, Aberdeen AB10 7GJ, UK
e-mail: e.gobina@rgu.ac.uk

S. Habiba
e-mail: h.shehu@rgu.ac.uk

O. Edidiong
e-mail: e.p.okon@rgu.ac.uk

S.-I. Ao et al. (eds.), *Transactions on Engineering Technologies*,
DOI 10.1007/978-981-10-1088-0_5

A Constant representing viscous flow
D Diffusivity (m^2 s^{-1})
D_g Diffusion coefficient
Ds Fick's diffusivity constant
N Flux (mol s^{-1} m^{-2})
M Gas molecular mass (g mol^{-1})
N_g Gas translational diffusion
K Knudsen number
S Membrane area (m^2)
R Molar gas constant (8.314 J mol^{-1} K^{-1})
Q Molar gas flow rate (mol s^{-1})
J Permeability (mol m m^{-2} s^{-1} Pa^{-1})
ΔP Pressure drop across the membrane (Pa)
d_p Pore diameter (m)
N_s Surface flux
D_o The intrinsic or corrected diffusivity
T Temperature (K)

Greek Symbols

Å Angstrom
μ_m Average velocity (m s^{-1})
λ Mean free path of gas molecule (m)
r_p Membrane Pore radius (m)
Γ Thermodynamic correction factor

1 Introduction

Gaseous hydrocarbons that are prevalent under increased pressure are solution gases in oil reservoirs. At equilibrium, they are in solution with the liquid hydrocarbon phase. These hydrocarbon gases are usually conserved but in some cases their storage is considered uneconomical and the gases are flared which is not an ideal practice. The impact of gas flaring cannot be over emphasized, it can cause detrimental effects to the environment [1], and these effects are highlighted below:

Emissions of methane and carbon dioxide: The main gases responsible for global warming are carbon dioxide and methane with methane being about 35 times more potent than carbon dioxide. The reduction of the volume of gases wasted by flaring without compromising oil production can be achieved by exploiting gas conservation opportunities [2].

Nitrous oxide emissions in the presence of volatile organic compounds: The emissions of nitrous oxides in the presence of volatile organic compounds can lead to the formation of ground level ozone which can have a toxic effect to the vegetation and humans as well. Nitrogen oxide is a major contributor to acid rain as well.

Sulfur dioxide and hydrogen sulphide emissions: Hydrogen sulfide is a corrosive toxic gas that can be oxidized rapidly to sulfur dioxide, which is a contributor to acid rain. Many efforts have been made in the last couple of years to develop an effective method for the separation and subsequent removal of impurities from natural gas.

There are ongoing researches on the use of nano-composite ceramic membranes to separate gaseous mixtures hence making it one of the emerging technologies that is growing fast. Their use has grown considerably both academically as well as industrially and they can be used for several applications. They are generally more expensive to fabricate than polymeric membranes but they can withstand more rigorous separation conditions that include high temperatures or corrosive solvents [3]. Ceramic membranes do not only have higher thermal and chemical stability but also have higher permeability as well [4]. There are several types of support used for these membranes. These include zeolites, silica, alumina and stainless steel [5]. The various use of ceramic membranes include hydrogen separation and purification to get ultra-pure hydrogen, recovery of CO_2 from natural gas and power station flue gases and oxygen or nitrogen enrichment of air [6, 7].

Ceramic membranes that are available commercially generally have a pore size of 5 nm or bigger [8]. With the modification of these ceramic membranes the pore size may be reduced to near molecular dimensions, enabling separation of components based on the differences in molecular sizes or in the shape of the components [9]. There are various methods that can be used for the modification including deposition that aims at the formation of porous or non-porous layer on the surface. Further processing by means such as annealing, carbonization or plasma treatment can follow the modification for further optimization. Examples of deposition techniques include: chemical vapor deposition (CVD), sol-gel deposition, Langmuir-Blodgett (LB) deposition, spin coating and self-assembly [3].

Gas permeation by Knudsen diffusion varies inversely with the square root of the molecular weights of the gases. Hence an ideal separation for a mixture of binary gases is equal to the inverse of the square root of their molecular mass ratio [10]. The transportation equation that comprises of Knudsen and viscous flow is given by:

$$J = A\bar{P} + B \tag{1}$$

According to Eq. (1), A is the constant representing viscous flow while B is the constant representing non-viscous flow, $\bar{P}$ is the average pressure across a membrane and J is the permeability of the membrane and it is calculated using the equation:

$$J = \frac{Q}{S} . \bar{P} \tag{2}$$

where Q is the flow rate in mol s^{-1} and S is the membrane area in m^2. The pore radius of the membrane can be determined using the formula [11]:

$$r_p = \frac{16 . A . \mu}{3 . B} \sqrt{8RT/\pi M} \tag{3}$$

where M is the molar mass of the gas (g mol^{-1}), R is the molar gas constant (8.314 mol^{-1} J K^{-1}), T is the temperature in (K) and μ is the viscosity (Pa s^{-1}) of the gas.

The Knudsen number is given by:

$$K = d_p/\lambda \tag{4}$$

where d_p is the pore diameter (m) and λ is the mean free path of the molecules (m). The Knudsen number determines the flow regime of the membrane. When the diameter of the pores is lower than the mean free path of the molecules then Knudsen flow is dominant [11]. The assumption made using this model is that there is negligible pressure drop due to the relatively small length of the capillaries [12].

Gas transport through α-Al_2O_3 support can involve both Knudsen and viscous flow when the interaction between the gas and the pore walls of a porous membrane is negligible [13]. A plot of gas permeability against the mean pressure drop is depicted in Fig. 1; this is for a membrane that is free of defects.

According to Fig. 1, the intercept B at the axis ordinate represents the contribution of Knudsen flow and in membrane 1 gas transport takes place in a region of Knudsen flow and thus for a defect free membrane, the gas permeability remains unchanged with increase in trans membrane mean pressure. The contribution due to viscous flow is represented by membrane 2 while membrane 3 is a representation of both Knudsen and viscous transport mechanism [13].

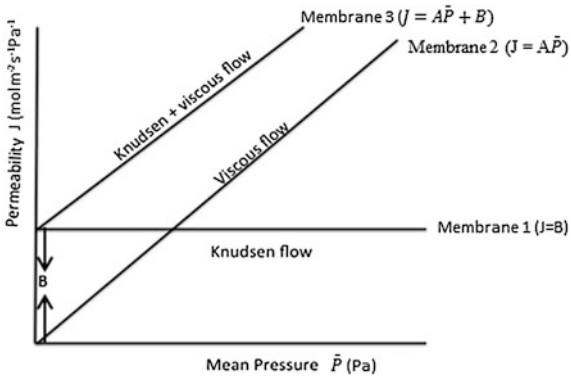

Fig. 1 The contributions of Knudsen diffusion and viscous flow [13]

For a commercial ceramic membrane, at elevated temperatures and low pressures the most likely transport mechanism employed is the Knudsen flow. Molecular sieving does not take place since the pore sizes are larger than the gas molecules [14]. The transport of gases through only Knudsen diffusion has been found to be inhibitive on the selectivity of a separating system. To overcome this difficulty, various efforts to promote other modes of transport have been made by surface modification [6]. The choice of membrane material greatly affects the permeation flux and selectivity of different gases as they move through the membrane [15]. In this research work the morphology of the silica and zeolite membrane was determined using the Scanning Electron Microscope (SEM).

The process of mass transport through a membrane varies for different membrane materials. For a zeolite layer gas transport is as a result of the following five steps [16, 17].

- Adsorption of the substance on the outer surface of the membrane
- Mass transport from the outer surface into the zeolite pore
- Diffusion through intra-crystalline zeolite
- Mass transport out of the zeolite pores to the external surface
- Desorption from the outer surface to the bulk.

Adsorption and desorption of the species from the outer surface of the zeolite layer depends on the permeation conditions (temperature and pressure), type of crystalline material and the nature of the chemical specie. Steps 2, 3 and 4 are usually activated processes [18].

Intra crystalline permeation through a zeolite membrane can be described using various approaches [19]. The Fickian approach uses the concentration gradient as the driving force in a membrane while for the Maxwell-Stefan (MS) approach the driving force is the gradient of the thermodynamic potential. The MS approach allows for the approximation of the flux through the membrane for multicomponent gas mixtures by using the information from single gas permeations [20]. For the permeation of single gas components through a zeolite membrane in a wide range of temperatures, the Fickian approach can be followed and the assumption that the total flux N is the combination of the surface flux N_s which takes place at low to medium temperatures and the activated gaseous flux N_g which is prevalent at high temperatures [16, 17, 21, 22].

$$N = N_s + N_g \tag{5}$$

2 Experimental

A schematic diagram of the membrane flow apparatus used for the permeation test for the gases is presented in Fig. 2. Four different gases: carbon dioxide, helium, nitrogen and argon were used for the permeability through a porous ceramic membrane at various trans-membrane pressures [22].

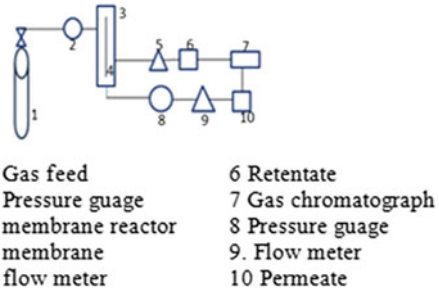

Fig. 2 Schematic diagram of a membrane permeation flow system

2.1 Preparation of the Silica Membrane

The dip coating method (Fig. 2) was used to modify the membrane. In this method, the support layer which comprises of a porous alumina which is dipped into a solution consisting of Silicone elastomer, curing agent and isopentane in the ratio 10:1:100 respectively. The mixture was first homogenized with magnetic stirring for 2 h before the support is dipped for 1 h with constant stirring to prevent the mixture from gelling. The membrane was air dried for 30 min and thermally treated at 333 K for 2 h prior to permeation test. The dip-coating set up is shown in Fig. 3 and the composition of the solution used for membrane modification is given in Table 1 [22].

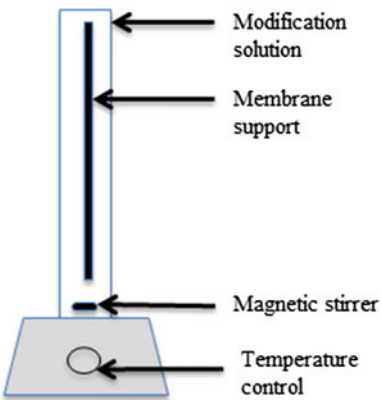

Fig. 3 Membrane modification using the dip-coating process

Table 1 Composition of the dip-coating modification solution

Silicone elastomer	50 ml
Curing agent	5 ml
Isopentane	500 ml

Table 2 Composition of the modification solution for zeolite membrane

Chemical	Amount (ml)
Aluminium oxide	10
Sodium hydroxide	14
Deionised water	798
Silicone oxide	1

2.2 Preparation of the Zeolite Membrane

For the zeolite membrane preparation, a solution containing silicone oxide, aluminium oxide, sodium oxide and deionized water was prepared and homogenized at room temperature for 20 h. The amount of each substance used is given in Table 2. Zeolite crystals were deposited on alumina support that is subsequently dipped into the solution and kept for 20 h at 343 K using a similar system as described in Fig. 3. The membrane was washed with deionized water and the pH of the rinse water was monitored. When the rinse water pH was neutral the membrane was air dried for 20 min and thermally treated in the oven at 338 K for 2 h prior to permeation test [22].

2.3 Membrane Characterization

The morphology of the membrane was determined by the use of the scanning electron Microscope (SEM) and the elemental composition of the membrane was confirmed using Energy Dispersive X-Ray Analysis (EDAX).

3 Results and Discussion

3.1 Gas Permeation of Silica Membrane

The gas flow rate through the silica membrane was used to calculate the permeance using Eq. (2) and the plot of permeance against the pressure drop is shown in Fig. 4.

It is observed that the permeance decreased with increase in feed pressure, CO_2 has the lowest permeance but the highest molecular weight and He has the lowest molecular weight but highest permeance, hence this follows an inverse relationship between molecular weight and permeance which follows the flow mechanism of Knudsen flow [16]. At pressures higher than 0.1 bar the plot indicate a flow that is consistent with Knudsen flow for a membrane that is free from defects as shown in Fig. 1. The order of molecular weights is $CO_2 > Ar > N_2 > He$. Nitrogen and argon have close permeance as can be observed in Fig. 4 but their molecular weights are not close. This could imply that a different flow mechanism was responsible for the transport of these gases across the membrane.

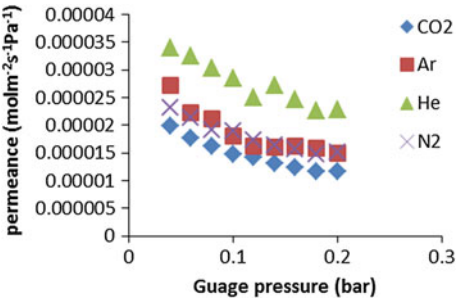

Fig. 4 Effect of pressure on gas permeance of silica membrane at 298 K

From Eqs. (1) and (3), the pore radius of the membrane was calculated.

The slope (A) of the graph is the viscous contribution, while the intercept (B) is the contribution due Knudsen flow. From Fig. 5, the pore radius and the mean free path of the molecules was calculated and represented in Table 3.

Theoretically the pore radius of the membrane is supposed to be the same and independent of the type of gas. However, as can be seen in Table 3, there is variation with He giving the highest value and CO_2 giving the lowest. Hence the membrane will have a distribution of pore sizes and different gases will flow through these pores at different rates depending on the resistance to flow. From Table 3, it can be seen that the calculated pore radius is much lower than the mean free path, which implies that the dominant flow of the gases is Knudsen flow.

In Table 4, the Knudsen selectivity was calculated using the square root ratios of the molecular weights of the gases. These are presented in Fig. 5 and compared with the pure gas selectivity values based on the permeability ratio.

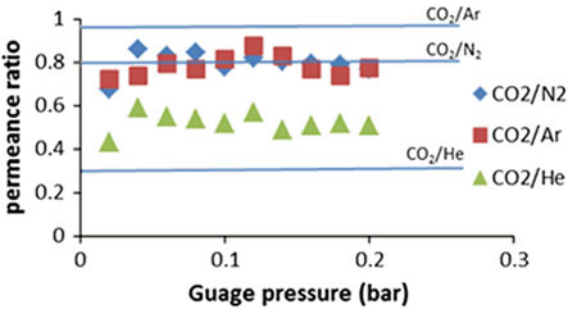

Fig. 5 Permselectivity with CO_2 at room temperature

Table 3 Pore radius of the membrane and mean free path of the gases

	rp(m)	λ(m)
Ar	0.037×10^{-10}	1.48×10^{-4}
He	0.312×10^{-10}	6.24×10^{-4}
N_2	0.044×10^{-10}	2.93×10^{-4}
CO_2	0.029×10^{-10}	1.99×10^{-4}

Table 4 Knudsen selectivity calculated using the molecular weights of the gases

Gases	Knudsen selectivity
CO_2/N_2	0.799
CO_2/Ar	0.952
CO_2/He	0.302

The Knudsen selectivity calculated has higher values for CO_2/Ar at all the pressures investigated than the experimental Knudsen selectivity calculated using the ratio of the gas permeability. This could indicate another flow mechanism should be employed for the separation of these gases. For CO_2/He, the Knudsen selectivity calculated is lower than the experimental value that could indicate a good separation of helium if this performance were to be replicated in a mixed gas stream.

A plot of the permeance against the inverse of the square root of the molecular weights of the gases is given in Fig. 6.

The graph is not linear as expected for Knudsen flow mechanism.

To further explain the flow mechanism that the membrane exhibited, Fig. 7 is a plot of gas permeance against the kinetic diameter of the gas molecules to see if the mechanism could be molecular sieving. According to Pandey and Chauhan [10] the smaller molecules will permeate while the larger molecules will be retained.

The order of the kinetic diameter of the gases starting from the largest is $N_2 > Ar > CO_2 > He$. It can be seen that nitrogen having the highest kinetic diameter is permeating at a rate that is higher than argon and carbon dioxide which both have lower kinetic diameters. Figure 7 proves that the membrane did not exhibit molecular sieving flow mechanism.

Nitrogen and argon have similar permeance although they possess different molecular weights. This could indicate there is a different flow mechanism that is responsible for the flow of these gases. The flux of nitrogen was determined and showed an increase in flux with the increase in temperature.

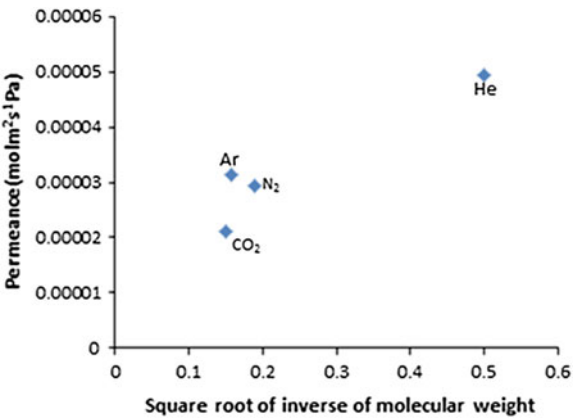

Fig. 6 Permeance against inverse of the square root of the molecular weights of the gases

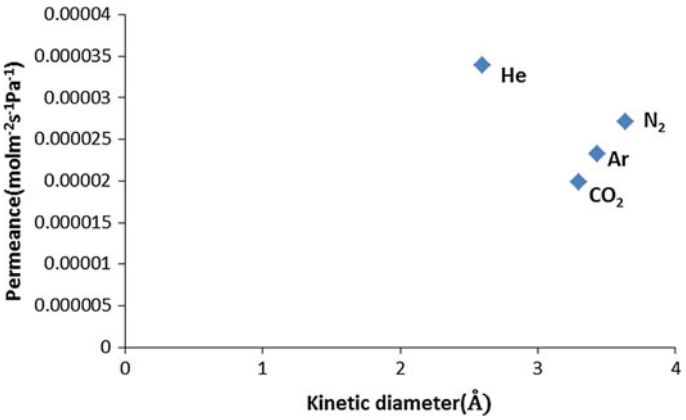

Fig. 7 Permeance at 298 K and 2 kPa against kinetic diameter

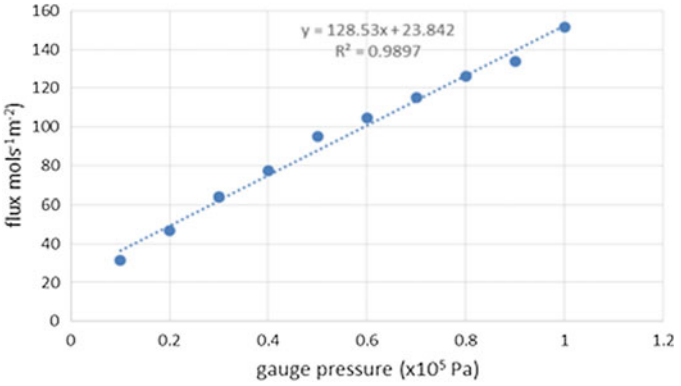

Fig. 8 Effect of gauge pressure on the flux of nitrogen at 298 K using silica layer

The flux of nitrogen as depicted in Fig. 8 increases linearly with increase in pressure, and it has a good correlation coefficient of 0.9897. The other gases (carbon dioxide, argon and helium) also had high fluxes at higher pressures.

3.2 Gas Permeation of Y-Type Zeolite Membrane

The flux of propane, nitrogen and methane was determined through the zeolite layer. Figure 9 depicts the flux of nitrogen and Fig. 10 shows the permeances of propane, nitrogen and methane against the gauge pressure.

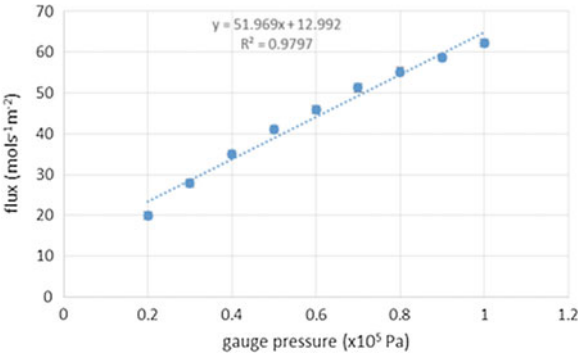

Fig. 9 Effect of gauge pressure on the flux of nitrogen at 298 K using zeolite layer

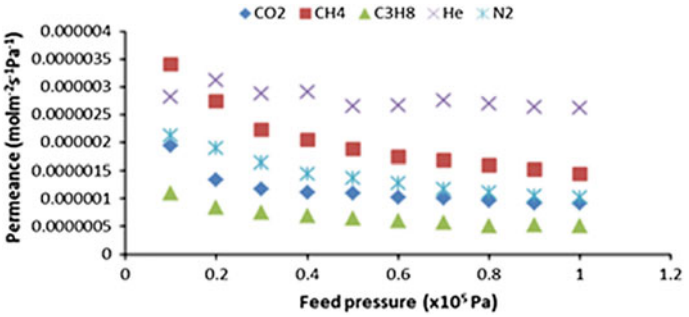

Fig. 10 Effect of pressure on gas permeance of zeolite membrane at 298 K

Compared to the plot in Fig. 4, the values fit more closely to membrane 1 where the permeance J = B as described in Fig. 1.

3.3 Membrane Characterization

The SEM images were collected in order to have an insight on the morphology of the selective layer. The cross section of the α–Al_2O_3 ceramic membrane support is shown in Fig. 11 and the surface of the synthesized membranes is shown Fig. 12a for the silica and Fig. 12b for the zeolite membrane.

The thickness of the membrane can be estimated as 6 ± 0.2 µm.

The images in Fig. 12 show the pore structure of the silica that is deposited on the aluminium support. Both the silica and zeolite are deposited on the support unevenly which could suggest that the pore size distribution could be unequal at different points of the membrane

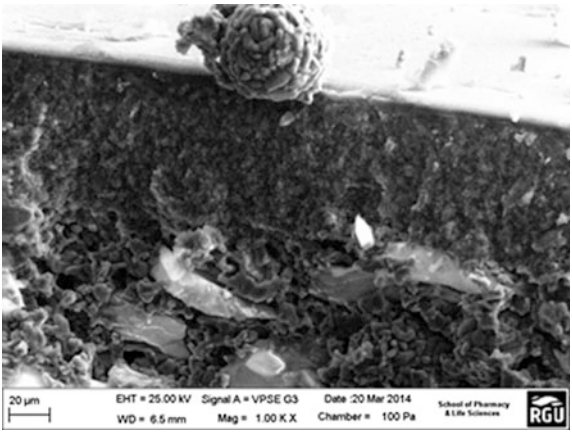

Fig. 11 Cross section image of α–Al_2O_3 membrane support

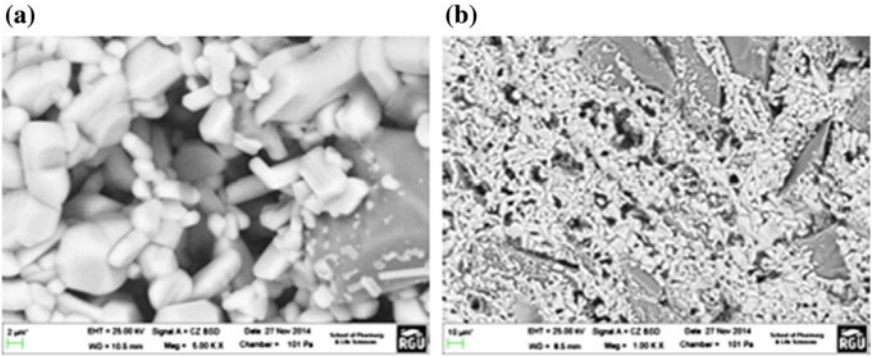

Fig. 12 The outer surface of silica (**a**) and zeolite (**b**) membrane

4 Conclusion

An investigation on gas separations efficiency of inorganic membranes has been carried out. The support was modified and the flow mechanism of the membrane was investigated. On the basis of the results obtained it can be concluded that the main mechanism governing the flow of gases through the modified silica membrane was Knudsen flow although there is evidence that another flow mechanism come to play. Further work will be carried out to determine how to modify a membrane support to achieve a specific flow mechanism. Studies from literature and preliminary experimental work have shown that for the separation of lower hydrocarbons, zeolite membranes have more efficacy than the silica or alumina ones. From the

SEM images observed there is a need to modify the deposition of pore modifying agents on a membrane support to achieve a defect free membrane with an even pore size distribution over the entire effective length of the membrane

Acknowledgements The conference was sponsored by IDEAS Research Institute, The Robert Gordon University Aberdeen, United Kingdom. The Authors of this paper acknowledge the center for Process Integration and Membrane Technology at RGU for providing the research infrastructure and the School of Pharmacy Life Science for the SEM/EDAX analysis.

References

1. Abedini R, Nezhadmoghadam A (2010) Application of membrane in gas separation processes: its suitability and mechanisms. Pet Coal 52(2):69–80
2. Tarmoon I (1999) Middle east oil show, 20–23 February
3. Schüth F, Sing KSW, Weitkamp J (2002) Handbook of porous solids. Wiley-Vch, Weinheim
4. Huang P, Xu N, Shi J, Lin Y (1997) Recovery of volatile organic solvent compounds from air by ceramic membranes. Ind Eng Chem Res 36(9):3815–3820
5. Li H, Schygulla U, Hoffmann J, Niehoff P, Haas-Santo K, Dittmeyer R (2013) Experimental and modeling study of gas transport through composite ceramic membranes. Chem Eng Sci 111:20
6. Baker RW (2000) Membrane technology. Wiley Online Library, New York
7. Powell CE, Qiao GG (2006) Polymeric CO_2N_2 gas separation membranes for the capture of carbon dioxide from power plant flue gases. J Membr Sci 279(1):1–49
8. Singh RP, Way JD, McCarley KC (2004) Development of a model surface flow membrane by modification of porous vycor glass with a fluorosilane. Ind Eng Chem Res 43(12):3033–3040
9. Van de Graaf JM, Kapteijn F, Moulijn JA (1999) Modeling permeation of binary mixtures through zeolite membranes. AIChE J 45(3):497–511
10. Pandey P, Chauhan R (2001) Membranes for gas separation. Prog Polym Sci 26(6):853–893
11. Julian A, Juste E, Chartier T, Del Gallo P, Richet N (2007) Catalytic membrane reactor: multilayer membranes elaboration. Catalytic membrane reactor: multilayer membranes elaboration. In: Proceedings of the 10th international conference of the european ceramic society, p 718–722
12. Gobina EN, Oklany JS, Hughes R (1995) Elimination of ammonia from coal gasification streams by using a catalytic membrane reactor. Ind Eng Chem Res 34(11):3777–3783
13. Li A, Zhao H, Gu J, Xiong G (1997) Preparation of γ-$A1_2O_3$ composite membrane and examination of membrane defects. Sci China B Chem 40(1):31–36
14. Sidhu PS, Cussler E (2001) Diffusion and capillary flow in track-etched membranes. J Membr Sci 182(1):91–101
15. Bernardo P, Drioli E, Golemme G (2009) Membrane gas separation: a review/state of the art. Ind Eng Chem Res 48(10):4638–4663
16. Burggraaf A (1999) Single gas permeation of thin zeolite (MFI) membranes: theory and analysis of experimental observations. J Membr Sci 155(1):45–65
17. Den Exter M, Jansen J, van de Graaf J, Kapteijn F, Moulijn J, Van Bekkum H (1996) Zeolite-based membranes preparation, performance and prospects. Stud Surf Sci Catal 102:413–454
18. Barrer RM (1990) Porous crystal membranes. J Chem Soc Faraday Trans 86(7):1123–1130

19. Krishna R, Van Baten J (2006) Describing binary mixture diffusion in carbon nanotubes with the Maxwell-Stefan equations. An investigation using molecular dynamics simulations. Ind Eng Chem Res 45(6):2084–2093
20. Basile A (2013) Handbook of membrane reactors: fundamental materials science, design and optimisation. Elsevier, UK
21. Xiao J, Wei J (1992) Diffusion mechanism of hydrocarbons in zeolites—I. Theory. Chem Eng Sci 47(5):1123–1141
22. Shehu H, Okon E, Gobina E (2015) The use of nano-composite ceramic membranes for gas separations. In: Proceedings of the world congress on engineering, London, UK, WCE 2015, 1–3 July 2015. Lecture Notes in Engineering and Computer Science, pp 1225–1229